



## Exploiting the conformational-selection mechanism to control the response kinetics of a "smart" DNA hydrogel

Journal:	<i>Analyst</i>
Manuscript ID	AN-ART-02-2018-000337.R1
Article Type:	Paper
Date Submitted by the Author:	05-Apr-2018
Complete List of Authors:	Simon, Anna; University of Texas, Austin, Center for Systems and Synthetic Biology; University of California Santa Barbara, Biomolecular Science and Engineering Walls-Smith, Luke; University of California, Santa Barbara, Department of Chemistry and Biochemistry Plaxco, Kevin W. ; University of California, Santa Barbara, California 93106-9510 United States, Biomolecular Science and Engineering; University of California, Santa Barbara, Department of Chemistry and Biochemistry; University of California, Santa Barbara, California 93106-9510 United States, Center for Bioengineering



Journal Name

ARTICLE

## Exploiting the conformational-selection mechanism to control the response kinetics of a “smart” DNA hydrogel

Received 00th January 20xx,  
Accepted 00th January 20xx

Anna J. Simon,<sup>a</sup> Luke T. Walls-Smith,<sup>b</sup> and Kevin W. Plaxco \*<sup>a, b, c</sup>

DOI: 10.1039/x0xx00000x

The sequence-specific hybridization and molecular recognition properties of DNA support the construction of stimulus-responsive hydrogels with precisely controlled crosslink geometry. Here we show that, as predicted by the conformational selection mechanism, the response kinetics of such a hydrogel can be tuned over orders of magnitude by modulating the thermodynamic stability of its crosslinks.

[www.rsc.org/](http://www.rsc.org/)

### Introduction

Materials that undergo physical or chemical transformations in response to specific molecular effectors are common in biology, and include muscle fibers,<sup>1</sup> squid iridophores,<sup>2</sup> and many viral capsids.<sup>3</sup> The design of similarly responsive artificial hydrogels has been an area of active study in recent years.<sup>4, 5, 6, 7, 8, 9</sup> To this end, researchers often turn to DNA as a substrate, as its modular, well-understood base-pairing rules support the construction of complex, precisely-articulated three-dimensional networks.<sup>7, 8, 9, 10</sup> These are rendered responsive to specific molecular cues via the incorporation of structure-switching aptamers, DNA sequences that can be engineered to undergo large-scale conformational changes upon binding to a specific molecular “effector,” as crosslinkers. The use of these enables the construction of DNA-based materials that assemble, dissolve, or reconfigure in response to diverse molecular targets including, for example, pH,<sup>11, 12</sup> specific oligonucleotide effectors,<sup>12</sup> metal ions,<sup>13, 14</sup> adenosine,<sup>14, 15</sup> thrombin,<sup>16</sup> PDGF,<sup>17</sup> ochratoxin A,<sup>18</sup> tumor cell-bound epithelial adhesion molecules,<sup>19, 20</sup> and sequence-specific endonucleases.<sup>21</sup>

An advantage of using aptamers as responsive crosslinkers in the design of smart materials is that DNA-DNA interactions are driven by well-understood, readily tuned base pairing interactions.<sup>22</sup> This suggests that the thermodynamics and kinetics of aptamer-crosslinked materials' responses to stimuli could, in theory, be tuned via simple sequence changes. To date, however, few studies of aptamer-based responsive

hydrogels have described the systematic, quantitative control of their properties,<sup>12, 15, 21</sup> and none have directly explored the relationship between the thermodynamic stability of the gel's crosslinking interactions and the kinetics with which it responds to its molecular effector. Motivated by this we explore here the effects of modulating crosslink stability on the responsiveness of a model DNA hydrogel.

### Experimental

#### Model system

As our model system we employed an adenosine-responsive variant of the well-established Y-DNA hydrogel architecture.<sup>9, 11, 15, 21</sup> This architecture consists of a mixture of two different trivalent, Y-shaped DNA “monomers” (each composed of three annealed strands) with pendant, single stranded arms that simultaneously hybridize to an aptamer sequence that serves as a crosslinker (Fig. 1A, Fig. SI. 1, 2). In the system we characterized here the two monomers hybridize to the 5' and 3' ends of an adenosine-binding aptamer (Fig. 1B),<sup>23</sup> forming an interconnected network appearing on the “macro” scale as a thick gel. This network dissolves upon the addition of sufficient concentrations of adenosine, as under these conditions the aptamer releases from the Y-monomers to bind this effector, breaking the gel's crosslinked structure (Fig. 1C). In contrast to shape-memory DNA-hydrogels<sup>10, 12, 13</sup> which contain permanent in addition to and target-responsive crosslinks and thus swell or shrink in response to stimuli, our model system contains entirely adenosine-responsive crosslinks and thus completely dissolves in response to sufficient concentrations of adenosine.

#### Measurement technique

<sup>a</sup>Biomolecular Science and Engineering Program, University of California Santa Barbara, Santa Barbara, CA 93106 USA

<sup>b</sup>Department of Chemistry and Biochemistry, University of California Santa Barbara, Santa Barbara, CA 93106 USA

<sup>c</sup>Center for Bioengineering, University of California Santa Barbara, Santa Barbara, CA 93106 USA

\*Current address: Center for Systems and Synthetic Biology, University of Texas Austin, Austin, Texas 78712

Electronic Supplementary Information (ESI) available: materials, methods, figures and code. See DOI: 10.1039/x0xx00000x

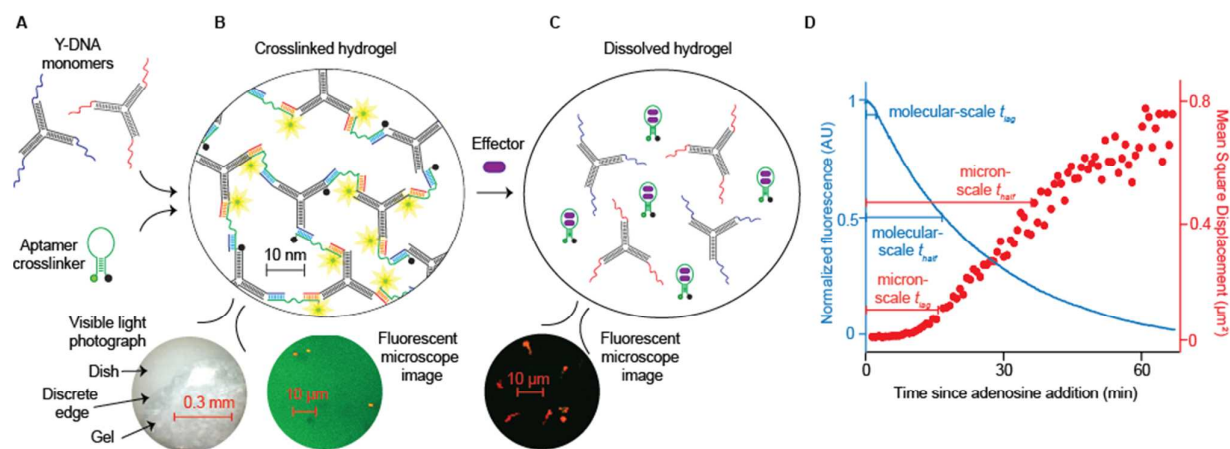


**Fig. 1.** (A) As our experimental system we employed an adenosine-responsive Y-DNA hydrogel containing Y-shaped “monomers” with pendant arms partially complementary to an adenosine-binding aptamer. (B) Hybridization to the aptamer crosslinks the monomers, forming a 3-dimensional network that appears as a visibly thick gel with discrete, solid-appearing edges (inset). (C) Upon the addition of adenosine the aptamer dissociates, dissolving the hydrogel. To monitor dissolution at the molecular length scale we employ a trace of fluorophore-quencher labelled aptamer that adopts an extended, fluorescent conformation when crosslinking monomers but a quenched stem-loop conformation upon binding adenosine. Tracer fluorescence thus scales with fraction of aptamer in its crosslinking conformation. To monitor dissolution at the micron length scale we employ the rheology of 1.0  $\mu\text{m}$  diameter polystyrene beads, which we embed in the gel by mixing with the Y-monomers prior to the addition of the aptamer crosslinker. The beads are trapped by the intact gel network but diffuse increasingly freely as the network dissolves.<sup>15</sup> To quantify this we filmed dissolution and determine the average change in the horizontal (i.e., left to right) position of beads between frames to define the one-dimensional Mean Square Displacement (MSD), a conventional metric of soft matter viscoelasticity.<sup>24</sup> (E) Upon the addition of effector the gel responds at both the molecular and micron length scales, with the observed dissolution at both length scales being biphasic, with a lag time,  $t_{\text{lag}}$ , followed by exponential decay with a characteristic time constant,  $\tau$ . Here we have defined the molecular and micron scale lag times, respectively, as the time required to reduce fluorescence by 5% from its initial value and for the mean square displacement of beads to equal 10% of the expected liquid-phase value. For comparison we also employ the half-life of dissolution,  $t_{\text{half}}$ , which is defined as the total time required to reduce fluorescence or increase bead diffusion to half way between the initial and final values. We visualize these transitions by averaging images over 20 frames ( $\sim 30$  s); intact gels show bright green background and little bead movement (B, inset, right); dissolved gels show dark background and substantial bead movement (C, inset). These inset plots do not represent quantitative measures of displacement, but serve as an efficient means to visualize mechanically rigid versus weak gels.

Although the gel-liquid transitions of responsive hydrogels are qualitatively apparent via visual inspection,<sup>9, 11, 12</sup> here we instead employ methods previously developed to quantitatively monitor the dissolution process as it occurs over a range of length scales (Fig. 1D).<sup>15</sup> We describe these methods briefly in the following paragraphs but in greater detail in our previous work.<sup>15</sup> To measure dissolution at the molecular length scale we employed a trace ( $\sim 1\%$ ) amount of aptamer modified with a fluorophore-quencher pair on its termini. This labelled tracer is highly fluorescent in its extended, crosslinking conformation (Fig. 1B) but quenched and dark in its dissociated, adenosine-bound conformation (Fig. 1C). To measure dissolution at micron length scale we employed the passive rheology of micron-diameter beads embedded in the gel which “jiggle” in place with Brownian motion with a mean square displacement proportional to the gel’s stiffness<sup>24</sup> (Fig. 1B-D). While traditional rheometer-based methods enable precise measurement of macroscale, equilibrium, mechanical properties (e.g., measurements of loss and storage moduli in refs<sup>12, 13</sup>), our passive rheology approach enables the simultaneous measurement of the gel’s micron scale properties and molecular-scale dissociation throughout the entire dissolution process. Our approach also enables a simple, visual means to qualitatively visualize intact versus dissolved gels. Highly crosslinked, mechanically strong gels, for example, fluoresce brightly and exhibit little bead movement in time-averaged images (Fig. 1D, left inset). More poorly crosslinked gels, in contrast, exhibit little fluorescence and substantial

bead motion in time-averaged images (Fig. 1D, right inset). Mixtures of Y-monomers in the absence of aptamer exhibit background levels of fluorescence and high bead motion (Fig. SI 3).

Using the above-described techniques we have previously<sup>15</sup> found that, in response to the sudden introduction of the effector, the adenosine-responsive Y-DNA hydrogel’s molecular and micron-scale dissolution kinetics are both bi-phasic, with a lag phase followed by a period of exponential dissolution (Fig. 1D).<sup>15</sup> To describe this quantitatively we have defined:<sup>15</sup> (1) the lag time,  $t_{\text{lag}}$ , as the time required to reduce fluorescence by 5% from its initial value (for molecular-scale dissolution) or as the time for the mean square displacement of beads to equal 10% of the expected liquid-phase value (for micron-scale dissolution); (2) a characteristic time constant,  $\tau$ , associated with the exponential decay seen after the lag phase; and (3) the half-life of dissolution,  $t_{\text{half}}$ , as the total time required to reduce fluorescence or increase bead diffusion to mid-way between their initial and final values. Data presented here are averages of at least three experimental replicates.

## Results

### Crosslinker permutations

In this work we studied the extent to which the gel’s crosslink density and dissolution kinetics vary with the thermodynamic stability of its crosslinking interactions. To do so we

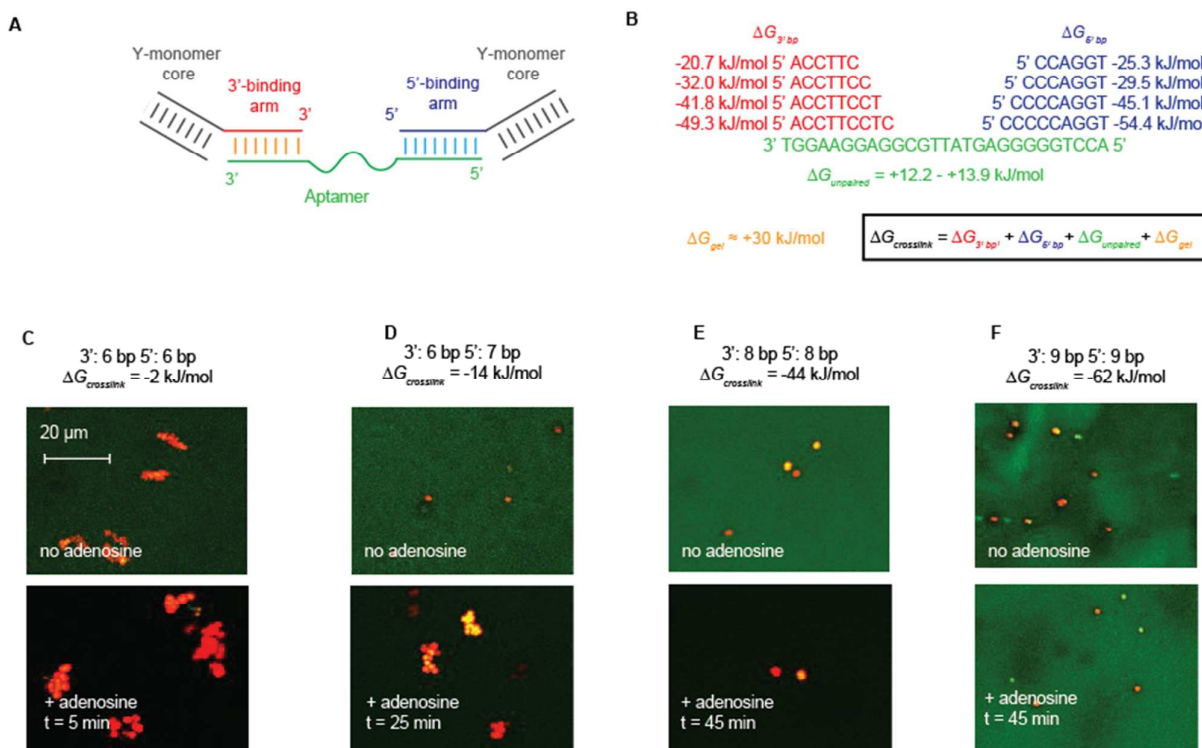


**Fig. 2.** (A) In our system, an adenosine-binding aptamer (green) crosslinks two Y-shaped monomers (shown in a larger-scale schematic in Fig. S1), whose pendant arms (red, blue) hybridize to varying lengths at the aptamer's 3' and 5' ends. (B) By varying the number of bases that each monomer binds to from 6 to 9 we produced 16 gel permutations ranging in predicted crosslink stabilities from -2 kJ/mol to -62 kJ/mol. (C-F) Crosslinking stability  $\Delta G_{crosslink}$  determines the permutation's ability to form, entrap beads, and respond to adenosine, which we assess by 20-frame (~30 s) averaged images of the gels before and long after addition of 10 mM adenosine; aptamer fluorescence is green and beads are red. For example, the permutation in which each monomer binds only six aptamer bases ( $\Delta G_{crosslink} = -2$  kJ/mol) exhibits moderate fluorescence and high bead motion even prior to the addition of effector, suggesting that its crosslink density is low. The permutation in which monomers bind 6 and 7 bases ( $\Delta G_{crosslink} = -14$  kJ/mol), in contrast, fluoresces brightly and entraps beads efficiently prior to the addition of effector. 25 minutes after the addition of 10 mM effector, however, this permutation is dark and exhibits rapid bead motion, indicating near complete dissolution. A more stable permutation, in which monomers bind eight bases on the two ends of the aptamer ( $\Delta G_{crosslink} = -44$  kJ/mol), is largely dissolved at the molecular level 45 minutes after the addition of effector, but exhibits little bead movement, indicating that it still remains crosslinked enough to entrap beads. Finally, the permutation in which monomers bind nine bases on the two ends of the aptamer ( $\Delta G_{crosslink} = -62$  kJ/mol) does not dissolve even at the molecular level 45 minutes after the addition of effector. In this highest-stability permutation, we consistently saw "patchy" fluorescence patterns, which we hypothesize to occur because the gel stiffness at these high crosslinking lengths prevents effective mixing upon aptamer addition. Control mixtures containing Y-monomers but no aptamer exhibit background levels fluorescence and bead mobility equivalent to those of the dissolved gels (see Fig. S1 3).

systematically varied the length of the single-stranded arms of each Y-DNA monomer such that they are complementary to 6, 7, 8, or 9 bases on each of the two ends of the aptamer. Taken together, these constructs produce 16 possible permutations, featuring total hybridization lengths of 12 to 18 base pairs (Fig. 2A, B). We incorporated these in hydrogels by annealing the relevant Y-monomer strands (the formation of which we validated via gel electrophoresis) stoichiometrically with the aptamer (SI methods, Fig. S1 1, 2). We estimated the crosslinker stability,  $\Delta G_{crosslink}$ , of each of the resulting hydrogels as the sum of the crosslinker's favourable base pairing (calculated using Mfold<sup>25, 26</sup>), an unfavourable term associated with constraining the unbound portion of the aptamer (calculated from excluded volume polymer theory<sup>27</sup>), and an unfavourable term associated with condensing the freely-translating components into a solid gel (measured in our previous work<sup>15</sup> as ~30 kJ/mol). From these estimates the predicted thermodynamic stabilities of the crosslinks we investigated vary from a marginally stable -2 kJ/mol (6 base

pairs on each side) to a very stable -62 kJ/mol (9 base pairs on each side).

#### Qualitative effects of $\Delta G_{crosslink}$ on gel stability and response

Even moderately enhanced crosslink stability promotes formation of mechanically strong gels. To see this we first qualitatively assessed the crosslinking density by the brightness of the fluorescence produced by the labelled tracer aptamers in their extended, crosslinking conformations, and the mechanical strength by the gel's ability to restrict the movement of micron-scale beads, comparing their positions over 30 s. The gel permutation based on the least stable crosslinks, in which the Y-monomers bind only six bases on each end of the aptamer, produces relatively little fluorescence, suggesting that its crosslinking density is only modest. This is consistent with the low estimated stability of this crosslink, which suggest that, at any given time, only 70% of the aptamers are bound to their complementary Y-

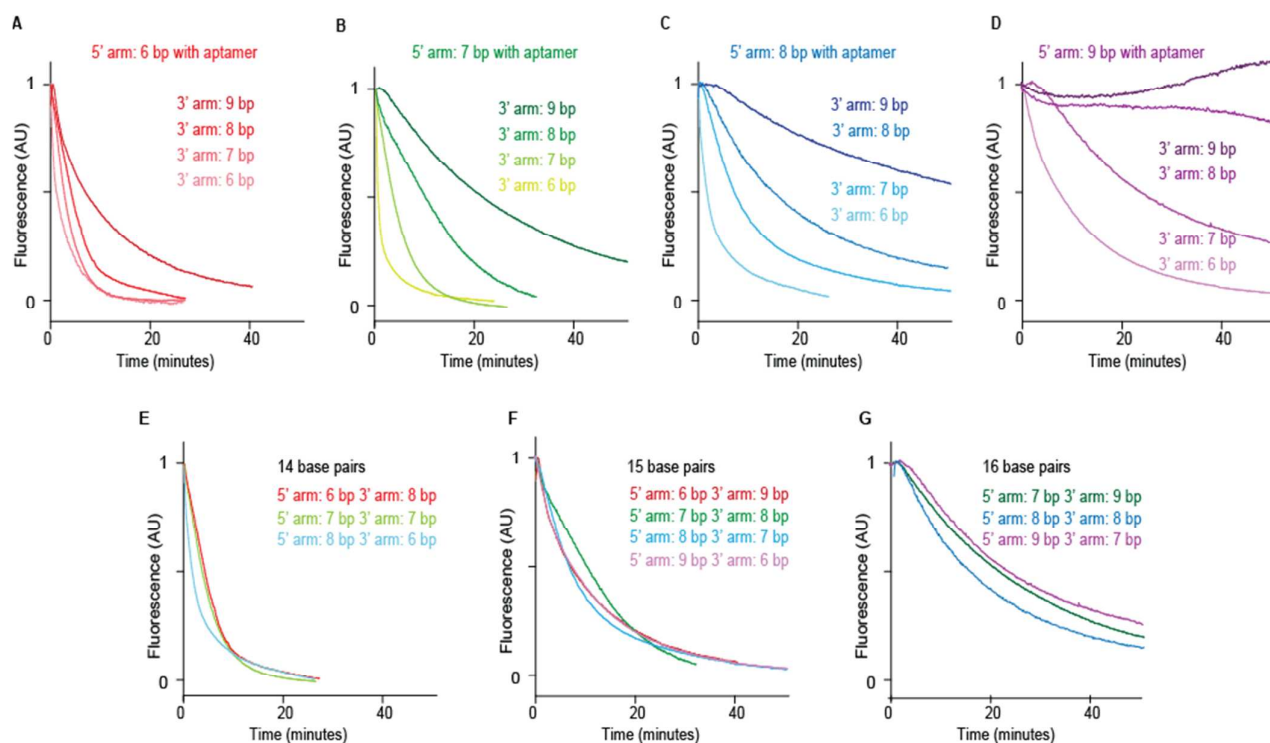


**Fig. 3.** We can finely tune the molecular-scale dissolution kinetics of our gel by changing the stability of its crosslinks. As shown, for example, increasing crosslink stability increases the time required for molecular-scale dissolution, as monitored by the fluorescence of a trace amount of fluorophore/quencher-modified aptamer. Panels A, B, C, and D show fluorescence-versus-time traces for gel permutations in which the monomer that binds the 5' end of the aptamer hybridizes with 6, 7, 8, or 9 bases, respectively, and the monomers binding the 3' end hybridizes to varying lengths of aptamer sequence. The time required for molecular-scale dissolution increases near-monotonically with increasing total hybridization length. Panels E, F, and G show fluorescence-versus-time traces for the permutations of monomers that bind a total of 14, 15, and 16 aptamer bases, respectively. The nearly identical fluorescence-versus-time traces for each of these given lengths suggests that for the permutations we have characterized, total base pairing length, rather than the distribution of base-pairing lengths between two sides of the aptamer, determine molecular-scale dissolution kinetics.

monomers. This level of crosslinking is so sparse that the gel fails to fully entrap beads, which move substantially even before the addition of adenosine (Fig. 2C). Increasing the aptamer/Y-monomer complementarity by one base pair on the 5' end (13 base pairs total; estimated crosslinking energy  $-14$  kJ/mol) significantly increases aptamer fluorescence, suggesting, not unreasonably, that this enhances crosslinking density. Correspondingly, measurements of bead motion show that this gel entraps beads quite effectively, with no apparent "jiggling" over the 30 s imaging window (Fig. 2C). This gel nevertheless responds rapidly to the addition of effector, with aptamer fluorescence decreasing to background levels and bead diffusion moving to free aqueous levels within  $\sim 5$  minutes after the addition of 10 mM adenosine (Fig. 2D).

Further increases in crosslink stability produce stiffer gels, but slow or even abolish the gel's response to its effector. Gels employing Y-monomers that bind eight and nine bases on each end of the aptamer (estimated crosslink energies of  $-44$  kJ/mol and  $-62$  kJ/mol, respectively) are highly fluorescent and entrap beads quite effectively, with no apparent motion over 30 s (Fig. 2E, F). And while the less stable of these two gels exhibits significant molecular scale dissolution in response to 10 mM adenosine (Fig. 2E), even after 45 min the gel retains sufficient crosslink density to entrap beads. The more stable of these two permutations, in contrast, does not exhibit detectable

molecular-scale dissolution, much less micron-scale dissolution, even 45 minutes after the addition of effector (Fig. 2F). This suggests that 10 mM adenosine does not outcompete the aptamer's affinity for the complementary Y-monomers employed in this gel, an observation that is consistent with our expectations: given that 10 mM is 4 orders of magnitude above the dissociation constant of the free aptamer,<sup>23</sup> the binding of effector at this concentration provides only  $-RT \ln(10^4) = -23$  kJ/mol and cannot outcompete the  $-62$  kJ/mol interaction energy of this highly stable crosslink.

#### Quantitative effect of $\Delta G_{\text{crosslink}}$ on response kinetics

Examining dissolution in more quantitative detail, we find that increasing crosslink hybridization (and thus stability) by even a single base pair lengthens the time required for molecular- (Fig. 3) and micron-scale (Fig. 4) dissolution. We visualized the relationship between base-pairing length and molecular-scale dissolution kinetics by plotting fluorescence-versus-time curves from permutations with the same 5' hybridization lengths and varying 3' hybridization lengths. These plots show a near-monotonic dependence between crosslink hybridization length and the gel's dissolution kinetics (Fig. 3A-D). The resultant slowing of the gel's response kinetics occurs via changes in both its lag and exponential phases. For

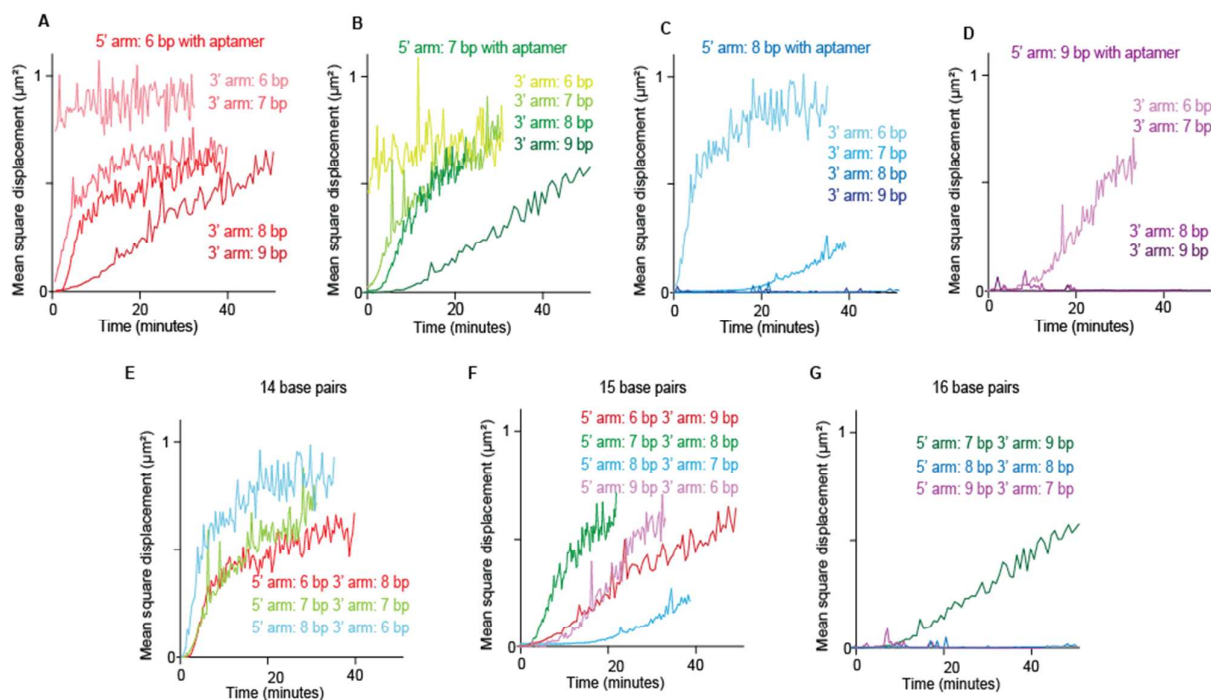


**Fig. 4.** As we observed for the gel's molecular-scale dissolution, its micron-scale dissolution time increases near-monotonically with increasing crosslink hybridization. Panels A, B, C, and D represent bead mean square displacement-versus-time traces for gel permutations in which the 5' end of the aptamer is hybridized to 6, 7, 8, or 9 bases of the monomer, respectively, and its 3' end is hybridized to sequences of varying length. Panels E, F, and G represent bead mean square displacement-versus-time traces for the permutations in which the crosslinking interactions contain a total of 14, 15, or 16 base pairs, respectively. Relative to dissolution at the molecular scale (Fig. 3), here we see larger (if still modest) variation in molecular-scale dissolution kinetics between these same-length permutations. We presume this reflects the relatively complex physics of phase transitions over longer length scales.

example,  $t_{lag}$ ,  $\tau$ , and  $t_{half}$  increase by 25 fold, 10 fold, and 13 fold, respectively, as we increase the total number of complementary bases in each crosslink from 12 to 16 (Fig. 5A-C).

Looking at the relationship between crosslink hybridization and the gel's response kinetics in more detail suggests that, on the molecular scale, total hybridization length is a more significant determinant of dissolution kinetics than the length of hybridization on either the shorter or longer arm. For example, all of the permutations of 14, 15, or 16 total base pairs produce nearly identical dissolution kinetics irrespective of how total hybridization length is distributed between the two arms (Fig. 3E-G).

The gel's micron-scale response kinetics qualitatively mirror those seen at the molecular scale. Plots of bead mobility-versus-time, for example, produce a similar, roughly monotonic increase in dissolution time with increasing hybridization length (Fig. 4A-D, Fig. 5D-E) with, once again, these effects apparent in both the lag and exponential phases. However, this said, however, the micron-scale dissolution behaviour of our gels varies much more between different permutations of the same total hybridization length than does molecular scale dissolution (Fig. 3, E-G, Fig. 4, E-G). We hypothesize that this arises from subtle differences in network geometry between permutations that changes the relationship between crosslinking density and micron-scale physical properties. Previous theoretical and experimental studies

demonstrate that this relationship between depends on spatial heterogeneity,<sup>28, 29, 30</sup> extent of chain entanglement,<sup>31, 32, 33</sup> and proportion of looped vs versus branched, tree-like topologies.<sup>35, 36, 37</sup> Notably, in dissolving gels, increased network entanglement<sup>32</sup> and tree-like compared to loop-like topologies<sup>37</sup> require a lower proportion of intact crosslinks to maintain mechanical strength. Given this, we suspect that the permutations with decreased micron- compared to molecular-scale dissolution may contain increased entanglement or loop topologies.

#### Conformational selection model

The extent to which a gel's response kinetics vary with the stability of its crosslinks is consistent with a conformational-selection model<sup>38, 39</sup> in which the dissolution rate depends on the proportion of the crosslinking aptamers that are in their "free," effector-binding conformation (i.e., are not bound to Y-monomers to form a double helix) at any given instant. This model predicts that the characteristic time constant associated with the exponential phase of dissolution,  $\tau$ , should scale with the rate with which the aptamer dissociates from the Y-monomer,  $k_{off, crosslink}$ .<sup>39</sup> Because the rate of aptamer-monomer association ( $k_{on, crosslink}$ ) is approximately constant over the hybridization lengths we measure,<sup>40</sup>  $\tau$  in turn varies with the stability of crosslinking,  $\Delta G_{crosslink}$ :

$$\tau \sim k_{off, crosslink} \sim e^{\Delta G_{crosslink}} \quad (1)$$

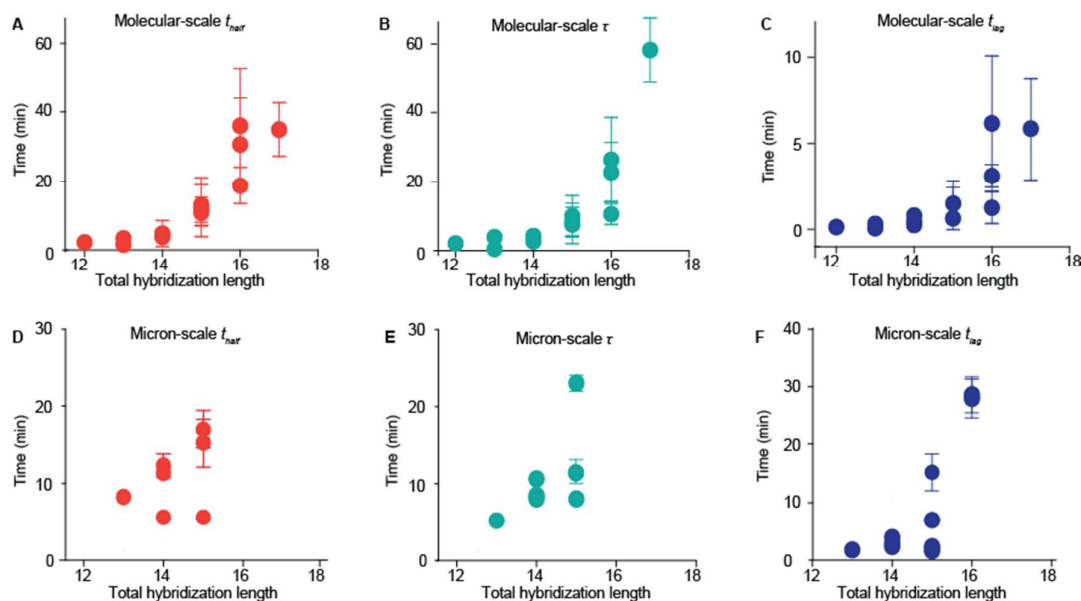


**Fig. 5.** To examine molecular-scale dissolution in quantitative detail we plot the molecular-scale time required to reduce fluorescence to half of its starting value,  $t_{half}$  (A), the timescale of the exponential phase  $\tau$  (B), and the lag time  $t_{lag}$  (C). Each of these molecular-scale parameters increases more-or-less monotonically with increasing crosslinking length. Plots of the equivalent micron-scale  $t_{half}$  (D),  $\tau$  (E) and  $t_{lag}$  (F) show that each of these parameters generally increases with increasing crosslinking hybridization length. However, the variability within a consistent hybridization length is considerably higher. Error bars represent standard errors of three separate measurements.

predicting a linear relationship between  $\ln(\tau)$  and  $\Delta G_{crosslink}$ :

$$\ln(\tau) \sim \Delta G_{crosslink} \quad (2)$$

Consistent with this prediction, a plot of  $\ln(\tau)$  versus  $\Delta G_{crosslink}$  produces a near linear relationship for molecular scale gel dissolution ( $R^2 = 0.9$ ; Fig. 6). For micron-scale dissolution, in contrast, this same plot produces a much weaker correlation ( $R^2 = 0.4$ ). While this may be due to the more complex physics associated with gel dissolution over these much longer length scales,<sup>29-37</sup> it could also arise due to fact that dissolution over this length scale is too slow for us to measure for the more stable crosslinks, reducing the total dynamic range that the model is attempting to capture (Fig. 6B).

## Conclusions

Here we demonstrate the ability to fine-tune the crosslink density and molecular- and micron dissolution kinetics of a molecularly responsive, aptamer-containing DNA hydrogel via modulation of thermodynamic stability of its crosslinks. Notably, we achieve this control by altering the structural elements to which the crosslinking aptamer binds rather than the aptamer itself, thus ensuring that the specificity of the gel for its effector remains unchanged.

Our results indicate a simple, predictable relationship between crosslinker stability and molecular- but not micron-scale behaviour. Detailed analysis of the molecular-scale

response suggests that crosslinker dissociation occurs via a conformational-shift mechanism, giving a simple, predictable

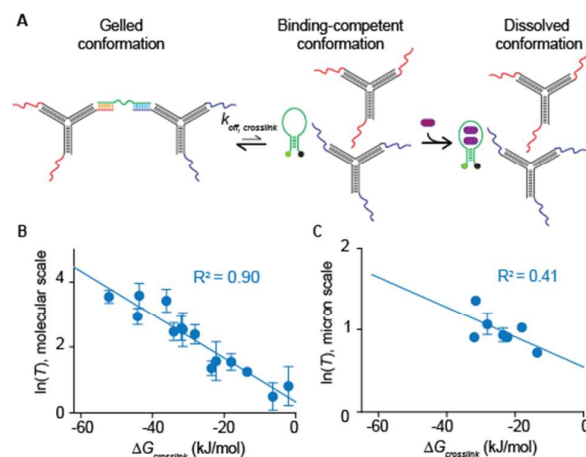


**Fig. 6.** The dependence of molecular- and micron-scale dissolution time constants,  $\tau$ , on crosslink stability supports a conformational selection model for dissolution.<sup>38, 39</sup> (A) In this model, aptamers equilibrate between their crosslinking conformation and their dissociated, effector-binding conformation even in the absence of the effector. The addition of effector traps the later population, driving the aptamer's conformational equilibrium to that state and concomitantly disrupting crosslinking. Quantitatively, this model predicts that the timescale of exponential dissolution  $\tau$  should scale with the spontaneous dissociation rate of individual crosslinkers,  $k_{off, crosslinker}$ . Assuming a relatively constant value of  $k_{on, crosslinker}$  (supported by previous experimental observations<sup>40</sup>) this relation predicts that  $\ln(\tau)$  should depend linearly with  $\Delta G_{crosslink}$ . (B) Consistent with this prediction,  $\ln(\tau)$  correlates linearly with  $\Delta G_{crosslink}$  ( $R^2 = 0.9$ ) for molecular-scale dissolution. (C) The correlation is poorer ( $R^2 = 0.41$ ) for micron-scale dissolution, likely due to the much poorer "baseline" from unmeasurably slow dissolution for very stable  $\Delta G_{crosslink}$  values, the more complex behaviour of dissolution over this much longer length scale dissolution, or both.

relationship between dissolution kinetics and crosslink thermodynamic stability. In contrast, however, while the micron-scale response generally slows with increasing crosslink length and stability, this relationship is more complex, with even permutations with identical crosslinking lengths and similar stabilities exhibiting varying behaviour. We hypothesize that this variability arises due to subtle differences in gel network architecture, potentially, for example, in the extent of looping and entanglement.

Our data suggest that while both molecular- and micron-scale stimulus-response properties may be readily controlled by tuning crosslinker stability and geometry, the relationship between them is complex. The relationship between molecular- and micron-scale materials is likely also complex in DNA-based materials with other network architectures, for example in shape-memory DNA hydrogels.<sup>12, 13</sup> Our results thus highlight the conventional wisdom that while engineering of synthetic biomolecular systems may readily provide materials optimal for arbitrary technological applications, bridging the gap from predictable molecular- to emergent-macroscale properties requires careful, perhaps empirical, observation.

### Conflicts of interest

There are no conflicts to declare.

### Acknowledgements

We thank M. Raven for training and technical support with imaging, T. Soh for the use of his facilities in the fabrication of the gel holder, and O. Saleh, M. Valentine, V. Gubala, M. Freddi, F. Fong, and J. Marquez for helpful discussions. L.T.W.-S. was supported by the Beckman Scholars program funded by the Arnold and Mabel Beckman Foundation. This work was funded by the Institute for Collaborative Biotechnologies through Grant No. W911NF-09-0001 from the U.S. Army Research Office. The content of the information does not necessarily reflect the position or the policy of the Government, and no official endorsement should be inferred. We also acknowledge the use of the NRI-MCDB Microscopy Facility and the multiphoton/laser scanning confocal microscopes supported by the NCRR and Office of the Director, National Institutes of Health of the NIH, under Award Nos. S10RR022585 and S10OD010610 respectively.

### Notes and references

- Farah, C. S., Reinach, F. C. The troponin complex and regulation of muscle contraction. *FASEB Journal*, 1995, **9**, 755-767.
- DeMartini, D. G., Izumi, M., Weaver, A. T., Pandolfi, E., Morse, D. E. Structures, organization, and function of reflectin proteins in dynamically tunable reflective cells. *J. Biol. Chem.*, 2015, **290**, 15238-15249.

- Zlotnick, A., Mukhopadhyay, S. Virus assembly, allostery, and antivirals. *Trends Microbiol.*, 2011, **19**, 14-23.
- Frazl, P., Barth, F. G. Biomaterial systems for mechanosensing and actuation. *Nature*, 2009, **462**, 442-44.
- Liu, K., Jiang, L. Bio-inspired design of multiscale structures for function integration. *Nanotoday*, 2011, **6**, 155-175.
- Montero de Espinosa, L., Meesorn, W., Moatsou, D., Weder, S. Bioinspired polymer systems with stimuli-responsive mechanical properties. *Chem. Rev.*, 2017, **117**, 12851-12892.
- Simmel, F. C., Schulman, R. Self-organizing materials built with DNA. *MRS Bulletin*, 2017, **42**, 913-919.
- Wang, D., Hu, Y., Liu, P., Luo, D. Bioresponsive DNA hydrogels: beyond the conventional stimuli responsiveness. *Acc. Chem. Res.*, 2017, **50**, 733-739.
- Hum, S. H., Lee, J. B., Park, N., Kwon, S. Y., Umbach, C.C., Luo, D. Enzyme-catalysed assembly of DNA hydrogel. *Nat. Mater.*, 2006, **5**, 797-801.
- Kahn, J.S., Hu, Y., Willner, I. Stimuli-responsive DNA-based hydrogels: From basic principles to applications. *Acc. Chem. Res.*, 2017, **50**, 680-690.
- Cheng, E., Xing, Y., Chen, P., Yang, Y., Sun, Y., Zhou, D., Xu, L., Fan, Q., Liu, D. A pH-triggered, fast-responding DNA hydrogel. *Angew. Chem. Int. Ed.*, 2009, **121**, 7776-7799.
- Ren, J., Hu, Y., Lu, C.-H., Guo, W., Aleman-Garcia, M.A., Ricci, F., Willner, I. pH-responsive and switchable triplex-based DNA hydrogels. *Chem. Sci.*, 2015, **6**, 4190-4195.
- Yu, X., Hu, Y., Kahn, J.S., Ceconello, A., Willner, I. Orthogonal dual-triggered shape-memory DNA-based hydrogels. *Chem. Eur. J.*, 2016, **22**, 14504-14507.
- Helwa, Y., Dave, N., Froidevaux, R., Samadi, A., Liu, J. Aptamer-functionalized hydrogel microparticles for fast visual detection of mercury(II) and adenosine. *ACS Appl. Mater. Interfaces*, 2012, **4**, 2228-2233.
- Simon, A.J., Walls-Smith, L.T., Freddi, M., Fong, F.Y., Gubala, V., Plaxco, K.W. Simultaneous measurement of the dissolution kinetics of responsive DNA hydrogels at multiple length scales. *ACS Nano*, 2017, **11**, 461-468.
- Zhang, L., Lei, J., Liu, L., Li, C., Lu, H. Self-assembled DNA hydrogel as switchable material for aptamer-based fluorescent detection of protein. *Anal. Chem.*, 2013, **85**, 11077-11082.
- Lai, J., Li, S., Shi, X., Coyne, J., Zhao, N., Dong, F., Mao, Y., Wang, Y. Displacement and hybridization reactions in aptamer-functionalized hydrogels for biomimetic protein release and signal transduction. *Chem. Soc.* 2017, **8**, 7306-7311.
- Liu, R., Huang, Y., Ma, Y., Jia, S., Gao, M., Li, J., Zhang, H., Xu, D., Wu, M., Chen, Y., Zhu, Z., Yang, Y. Design and synthesis of target-responsive aptamer-cross-linked hydrogel for visual quantitative detection of ochratoxin A. *ACS Appl. Mater. Inter.* 2015, **7**, 6982-6990.
- Song, P., Ye, D., Zuo, X., Li, J., Wang, J., Liu, H., Hwang, M. T., Chao, J., Su, S., Wang, L., Shi, J., Wang, L., Huang, W., Lal, R., Fan, C. DNA hydrogel with aptamer-toehold-based recognition, cloaking, and decloaking of circulating tumor cells for live cell analysis. *Nano Lett.*, 2017, **17**, 5193-5198.
- Li, S., Gaddes, E.R., Chen, N., Wang, Y. Molecular encryption and reconfiguration for remodeling of dynamic hydrogels. *Angew. Chem. Int. Ed.*, 2015, **54**, 5957-5961.
- Xing, Y., Cheng, E., Yang, Y., Chen, P., Zhang, T., Sun, Y., Yang, Z., Liu, D. Self-assembled DNA hydrogels with designable thermal and enzymatic responsiveness. *Adv. Mater.*, 2010, **23**, 1117-1121.
- Vallée-Bélisle, A., Ricci, F., Plaxco, K.W. Thermodynamic basis for the optimization of binding-induced biomolecular switches and structure-switching biosensors. *Proc. Natl. Acad. Sci. USA*, 2009, **106**, 13802-13807.

- 23 Huizenga, D.E., Szostak, J.W. A DNA aptamer that binds adenosine and ATP. *Biochemistry*, 1995, **34**, 656-665.
- 24 Crocker, J.C., Valentine, M. T., Weeks, E. R., Gisler, T., Kaplan, P. D., Yodh, A. G., Weitz, D. A. Two-point microrheology of inhomogenous soft materials. *Phys. Rev. Lett.*, 2000, **85**, 888.
- 25 SantaLucia, J.R. A unified view of polymer, dumbbell, and oligonucleotide DNA nearest-neighbor thermodynamics. *Proc. Natl. Acad. Sci. USA* 1998, **95**, 1460-1465.
- 26 Zuker, M. Mfold web server for nucleic acid folding and hybridization prediction. *Nucl. Ac. Res.*, 2003, **31**, 3406-3415.
- 27 Chan, H.S., Dill, K.A. Intrachain loops in polymers. *J Chem. Phys.*, 1989, **90**, 492-509.
- 28 Sakai, T., Katashima, T., Matsushita, T., Ching, U-I. Sol-gel transition behavior near critical concentration and connectivity. *Polymer Journal*, 2016, **48**, 629-634.
- 29 Zhong, M., Wang, R., Kawamoto, K., Olsen, B.D., Johnson, J.A. Quantifying the impact of molecular defects on polymer network elasticity. *Science*, 2016, **353**, 1264-1268.
- 30 Saalwächter, K., Seiffert, S. Dynamics-based assessment of nanoscopic polymer-network mesh structures and their defects. *Soft Matter*, 2018, **14**, 1976-1991.
- 31 Yang, Q.-S., Ma, L.-H., Shang, J.-J. The chemo-mechanical coupling behavior of hydrogels incorporating entanglements of polymer chains. *Int J. Sol. Struct.*, 2013, **50**, 2437-2448.
- 32 Nöll, T., Schönherr, H., Wesner, D., Schopferer, M., Paululat, T., Nöll, G., Construction of three-dimensional DNA hydrogels from linear building blocks. *Angew. Chemie*, 2014, **53**, 8328-8332
- 33 Ma, L., Yang, Q., Yang, C. Effects of the junction functionality and chain entanglements in chemomechanical behavior of polyelectrolyte gels. *Adv. Condens. Matt. Phys.*, 2015, 34580.
- 34 Kawamoto, K., Zhong, M., Wang, R., Olsen, B.D., Johnson, J.A. Loop versus branch functionality in model click hydrogels. *Macromolecules*, 2015, **48**, 8980-8988.
- 35 Wang, R., Lin, T.-S., Johnson, J., Olsen, B.D. Kinetic Monte Carlo simulation for quantification of the gel point of polymer networks. *ACS Macro. Lett.*, 2017, **6**, 1414-1419.
- 36 Lin, T.-S., Wang, R., Johnson, J.A., Olsen, B.D. Topological structure of networks formed from symmetric four-arm precursors. *Macromolecules*, 2018, **51**, 1224-1231.
- 37 Wang, J., Lin, T.-S., Gu, Y., Wang, R., Olsen, B.D., Johnson, J.A. Counting secondary loops is required for accurate prediction of end-linked polymer network elasticity. *ACS Macro. Lett.*, 2017, **7**, 244-249.
- 38 Ma, B., Kumar, S., Tsai, C.-J., Nussinov, R. Folding funnels and binding mechanisms. *Protein Eng. Des. Sel.*, 1999, **12**, 713-720.
- 39 Moal, I.H., Bates, P.A. Kinetic rate constant prediction supports the conformational selection mechanism of protein binding. *PLoS Comp Biol.*, 2012, **8**, e1002351.
- 40 Howorka, S., Movileau, L., Braha, O., Bayley, H. Kinetics of duplex formation for individual DNA strands within a single protein nanopore. *Proc. Nat. Acad. USA.*, 2001, **98**, 12996-13001.